ACS APPLIED MATERIALS & INTERFACES

Letter

www.acsami.org

Mediating the Contradiction of d_{33} and T_C in Potassium–Sodium Niobate Lead-Free Piezoceramics

Xiaojing Cheng,[†] Jiagang Wu,*[,†] Xiaopeng Wang,[†] Binyu Zhang,[†] Xiaojie Lou,[‡] Xiangjian Wang,[‡] Dingquan Xiao,[†] and Jianguo Zhu[†]

[†]Department of Materials Science, Sichuan University, 610064, P. R. China

[‡]Multi-disciplinary Materials Research Center, Frontier Institute of Science and Technology, Xi'an Jiaotong University, Xi'an 710054, P. R. China

ABSTRACT: For potassium–sodium niobate, the piezoelectric constant (d_{33}) was usually improved by sacrificing the Curie temperature (T_C). In this work, a material system of $0.992(K_{0.46}Na_{0.54})_{0.965}Li_{0.035}Nb_{1-x}Sb_xO_3$-$0.008BiScO_3$ has been designed and prepared with the aim of achieving both a large d_{33} and a high T_C at the same time. The chemical compositions are found to be homogeneously distributed in the ceramics. The introduction of Sc is found to be responsible for different grain sizes. The rhombohedral-tetragonal phase coexistence zone lies in the composition range of $0.02<x \leq 0.06$. The ceramic is thermally stable in terms of ferroelectric properties. The change in the domain-wall activities induced by the configuration variation of defect dipoles upon annealing is believed to be responsible for the variation in the d_{33} at different temperatures. The ceramic with $x = 0.025$ shows a good comprehensive performance of $d_{33} \approx 325$ pC/N and $k_p \approx 48\%$, together with a high T_C of ~358 °C, demonstrating that this material system is a promising candidate for high-temperature piezoelectric applications.

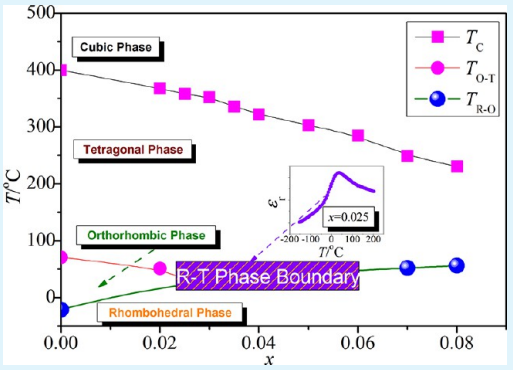

KEYWORDS: *lead-free piezoelectrics, R-T phase boundary, piezoelectricity, high Curie temperature*

INTRODUCTION

$Pb(Zr,Ti)O_3$ (PZT) ceramics have been widely used for the commercial products because of their excellent piezoelectric properties and high Curie temperature (T_C).[1−3] Unfortunately, the lead element involved in PZT is harmful for the surrounding environment, which will make PZT be prohibited in the near future due the environmental concern. Recently, extensive researches have been conducted for lead-free piezoelectric materials with a perovskite structure. A few candidate materials have been chosen for different practical applications,[4−23] for example, $(K,Na)NbO_3$ (KNN), $Bi_{0.5}Na_{0.5}TiO_3$, and $BaTiO_3$. Among all those materials, considerable attention has been given to the alkali niobate systems because of their large piezoelectric constant (d_{33}) and high T_C.[7−9,11,12,18−23] The research on lead-free piezoceramics is further boosted by the paper of Saito et al. published in 2004. They reported that the textured $(K,Na,Li)(Nb,Sb,Ta)O_3$ ceramics show excellent piezoelectric properties,[7] which has raised a broad interest on lead-free piezoceramics in the community.

The addition of ABO_3-type perovskites has been regarded as one of the most useful methodologies to improve the piezoelectric properties of KNN ceramics.[24−31] The monoclinic $BiScO_3$ can be prepared under a harsh condition of both a high pressure and a high temperature (6 GPa, 1400 K).[32] It was also found that a high piezoelectric activity can be achieved in KNN by forming its solid solutions with other perovskites, such as $PbTiO_3$.[33] Recent results also show that adding $BiScO_3$ can effectively enhance the piezoelectric properties of the KNN-based ceramics by forming the R-O or O-T phase boundary,[26−31] as shown in Table 1. For example, Zuo et al.[26] reported that the addition of $BiScO_3$ induces the formation of the R-O phase boundary in KNN, resulting in an improved d_{33}. KNN ceramics doped with Li^+ and $BiScO_3$ show both a high T_C of ~402 °C and a low d_{33} of ~225 pC/N.[31] The parameters for the KNN-based ceramics doped with $BiScO_3$ are listed in Table 1. From Table 1, it can be clearly seen that d_{33} and T_C highly contradict with each other. And a large d_{33} is normally obtained by sacrificing T_C.[26−31] As a result, it is highly desired to explore the possibility that whether a large d_{33} and a high T_C can both be obtained by fine tailoring the material system and constructing a new phase boundary in the KNN-based system.

To achieve both a large d_{33} and a high T_c in the KNN system, the material system of $0.992(K_{0.46}Na_{0.54})_{0.965}Li_{0.035}Nb_{1-x}Sb_xO_3$-$0.008BiScO_3$ ($KNLNS_x$-BS) has been designed and prepared in this work. The reasons for choosing the material system of $KNLNS_x$-BS are as follows. In this material system, adding $BiScO_3$ can decrease T_{O-T} and increase T_{R-O} of KNN.[26] Adding Li^+ not only improves T_C but also decreases T_{O-T} as well as the

Received: August 16, 2013
Accepted: October 18, 2013
Published: October 25, 2013

Table 1. Electrical Properties of $BiScO_3$-Modified KNN-Based Ceramics

material system	d_{33} (pC/N)	k_p	T_c (°C)	ref
0.98 $(Na_{0.5}K_{0.5})NbO_3$-0.02$BiScO_3$	210	0.45	350	Zuo[26]
0.98$K_{0.5}Na_{0.5}NbO_3$-0.02$BiScO_3$+Mn	288	0.46	328	Li[27]
0.992(0.95$K_{0.5}Na_{0.5}NbO_3$-0.05$LiSbO_3$)-0.008$BiScO_3$	305	0.54	315	Jiang[28]
0.985$(K_{0.48}Na_{0.52})(Nb_{0.98}Sb_{0.02})O_3-0.015BiScO_3$−$MnCO_3$	265	0.51	402	Wang[29]
0.995(0.95$K_{0.5}Na_{0.5}NbO_3$-0.05$LiSbO_3$)-0.005$BiScO_3$	280	0.49	~340	Li[30]
0.99$(Na_{0.485}K_{0.485}Li_{0.03})NbO_3-0.01BiScO_3$	225	0.38	402	Sun[31]
0.992$(K_{0.46}Na_{0.54})_{0.965}Li_{0.035}Nb_{1-x}Sb_xO_3-0.008BiScO_3$	325	0.48	~358	this work

sintering temperature. Besides, adding Sb^{5+} further suppresses the formation of the O phase.[34,35] The schematic diagram for the function of adding Li^+, Sb^{5+}, and $BiScO_3$ is shown in Figure.1. In this way, a new phase boundary showing the rhombohedral-tetragonal (R-T) phase coexistence has been developed. The ceramic with a specific composition prepared in this work has demonstrated both a larger d_{33} of ~325 pC/N and a high T_C of ~358 °C. In addition, the evolution of the microstructure with the doping Sb concentration is also clearly illuminated, and the related physical mechanisms for the enhanced electrical properties are given.

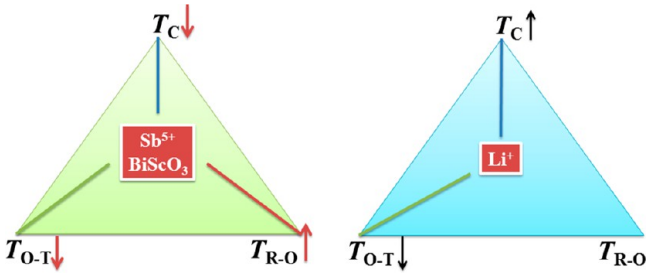

Figure 1. Schematic diagram of the effect of Li^+, Sb^{5+}, and $BiScO_3$ on T_C, T_{O-T}, and T_{R-O} of KNN.

EXPERIMENTAL SECTION

The material system of $0.992(K_{0.46}Na_{0.54})_{0.965}Li_{0.035}Nb_{1-x}Sb_xO_3-0.008BiScO_3$ with $0 \le x \le 0.08$ was prepared using the conventional solid-state method. Raw materials in this work were Na_2CO_3, K_2CO_3, Li_2CO_3, Nb_2O_5, Bi_2O_3, Sc_2O_3, and Sb_2O_3, respectively. The weighed powders were milled using the ethanol for 24 h, and then calcined at 850 °C for 6 h. These presintered powders were ball milled again and pressed into the pellets with 1.0 cm in diameter and ~1.0 mm in thickness. These pellets with x = 0, 0.02, 0.025, 0.03, 0.035, 0.04, 0.05, 0.06, 0.07, and 0.08 were sintered at 1065, 1070, 1075, 1075, 1080, 1085, 1090, 1095, 1100, and 1105 °C for 3 h in air, respectively. The silver paste was coated on both sides of the sintered samples, and then sintered at 650 °C for 10 min for electrical measurements. The samples were polarized at 30 °C in a silicone oil bath by applying a dc field of 3.0−4.0 kV/mm for 20 min.

X-ray diffraction with a CuK_a radiation (DX-2700, Dandong, P. R. China) has been used to characterize the phase structure of the sintered samples. Their microstructure, element mapping, and composition analysis were measured and recorded by a field-emission scanning electron microscope (FE-SEM) (JSM-7500, Japan). The temperature-dependent dielectric properties of the sintered samples were measured using an *LCR* analyzer (HP 4980, Agilent, U.S.A.) at a temperature range between −150−200 °C and room temperature~550 °C. The dielectric properties of the polarized samples were measured at 100 kHz, and the polarization vs electric field (P−E) hysteresis loops of the unpolarized samples were measured at 10 Hz using a ferroelectric tester (Radiant Technologies, Inc. Albuquerque, NM, USA). The planar electromechanical coupling factor (k_p) was measured by a resonance-antiresonance method with an impedance analyzer (Impedance Analyzer, PV70A, Beijing, P. R. China), and the d_{33} was measured using a commercial Berlincourt-type d_{33} meter (ZJ-3A, P. R. China) for the polarized samples. The thermal stability was measured by holding the polarized samples at different temperatures for 60 min, and all their d_{33} values are then measured after the sample cools down to room temperature.

RESULTS AND DISCUSSION

The room-temperature XRD patterns of the KNLNS$_x$-BS ceramics are shown in Figure 2a. A pure perovskite phase can

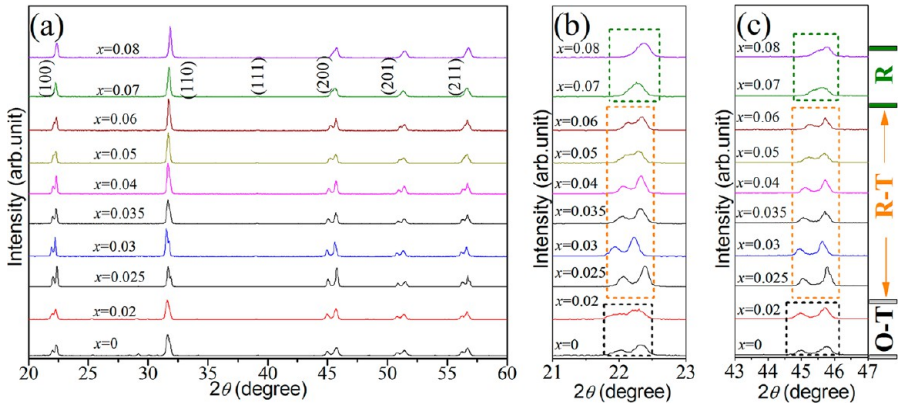

Figure 2. XRD patterns of the KNLNS$_x$-BS ceramics in the 2θ range of (a) 20−60°, (b) 21−23°, and (c) 43−47°.

be observed in all the ceramics except the sample with $x = 0$, indicating that doping Sb into the ceramics can result in the formation of stable solutions. Panels b and c in Figure 2 show the expanded XRD patterns of the KNLNS$_x$-BS ceramics, measured at $2\theta = 21-23°$ and $43-47°$. By considering the XRD data and the temperature-dependent dielectric constant (ε_r) (see Figures 3 and 4), the evolution in the phase diagram

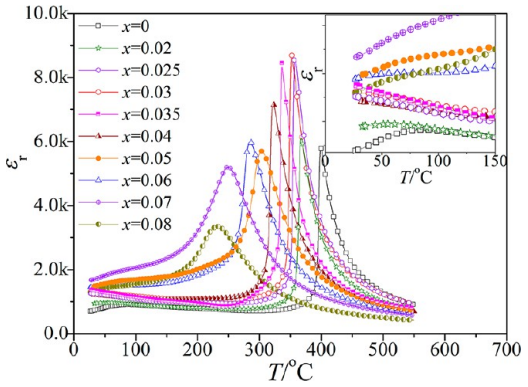

Figure 3. Temperature dependence of the dielectric constant of the KNLNS$_x$-BS ceramics. The inset shows the expanded ε_r–-T curves in the temperature range of 30–550 °C.

of the KNLNS$_x$-BS ceramics with x is analyzed, which is explained below: The O-T phase coexists at a specific temperature for the ceramics with $x \leq 0.02$,[36] and the $T_{O\text{-}T}$ of the ceramics with $x = 0$ and 0.02 is ~71 °C and ~52 °C (see Figure 3), respectively. In Figure 3, the dielectric constant (ε_r) of the ceramics with $x > 0.02$ gradually increases as the measurement temperatures drop from 150 °C to room temperature, indicating the existence of the phase boundary to some extent. It has been reported that doping Sb ions can simultaneously shift the R-O and O-T phase boundaries close to room temperature.[34] In addition, adding $BiScO_3$ can further shift the R-O and O-T to room temperature quickly.[26] In contrast, one can see from panels b and c in Figure 2,that the ceramics with $x \geq 0.07$ have a different phase structure. It has been reported that excessive Sb gives rise to an R phase above room temperature,[34] and thus the R phase is observed in these ceramics with $x \geq 0.06$. Finally, the R-T phase boundary of the ceramics has been defined in the x range of 0.02–0.06. It is of great interest to note that the XRD peaks shift to higher angles with increasing the Sb content, indicating a slight shrinkage of the lattice because of the substitution of Nb^{5+} ($R_{Nb} \approx 0.64$ Å) by Sb^{5+} ($R_{Sb} \approx 0.61$ Å).[34,37]

The effects of the Sb content on the phase transition of the KNLNS$_x$-BS ceramics was systematically studied using the temperature dependence of ε_r in the temperature range of −150 to 550 °C. Figure 3 shows the curves of ε_r versus temperature in the KNLNS$_x$-BS ceramics, characterized at 100 kHz and in the temperature range of 30 to 550 °C. There are two dielectric peaks for the ceramics with $x \leq 0.02$, which are attributed to the orthorhombic-tetragonal phase transition temperature ($T_{O\text{-}T}$) and the tetragonal-cubic phase transition temperature (T_C), as shown in Figure 3. So, the dielectric results are consistent with the XRD analysis (see Figure 2), confirming the involvement of the O-T phase boundary. However, the phase transition from an orthorhombic to a tetragonal phase gradually disappears above room temperature as the Sb doping level increases ($x > 0.02$), and there is only one peak left, which corresponds to the cubic-tetragonal phase transition at T_C. To clearly show the phase evolution with the Sb doping level, the temperature-dependent ε_r of the KNLNS$_x$-BS ceramics in a temperature range of −150 to 200 °C is shown in Figure 4a. $T_{R\text{-}O}$ and $T_{O\text{-}T}$ gradually move to room temperature as the Sb doping level increases,[34] and eventually they overlap with each other at room temperature, implying that the R-T phase boundary forms in the composition range of $x = 0.025$ and 0.05. Finally, an R phase appears in the ceramic with $x = 0.07$, which could be clearly seen by inspecting both the XRD pattern and the temperature -dependent ε_r. According to the temperature-dependent ε_r in Figures 3 and 4a, the phase diagram has been established, as shown in Figure 4b. T_c decreases almost linearly as the Sb content increases. $T_{R\text{-}O}$ and $T_{O\text{-}T}$ converge at room temperature for $0.02 < x \leq 0.06$. The $T_{R\text{-}O}$ of the ceramics with $x \geq 0.06$ shifts to above room temperature. As a result, the ceramics with the composition of $0.02 < x \leq 0.06$ are expected to show the R-T phase boundary lying around room temperature.

Figure 5a–d show the FE-SEM surface micrographs of the sintered samples with $x = 0$, 0.025, 0.05, and 0.07. One can see that the grain size is very sensitive to the Sb content in the KNLNS$_x$-BS ceramics. Also, different grain growth modes have been observed for the ceramics with different Sb contents, as shown in Figures 5a–d. Adding a small amount of Sb ($x < 0.05$) can promote the grain growth to some extent, while the grain size drops dramatically for $x \geq 0.05$ because of the involvement of excessive Sb.[34] In addition, the ceramics with $x = 0$ and 0.025 show a bimodal distribution of grain size together with a much larger grain size. The grain size decreases as the Sb doping level increases ($x \geq 0.05$). The ceramics with $x = 0$ and 0.025 show a much denser microstructure than those with $x \geq$

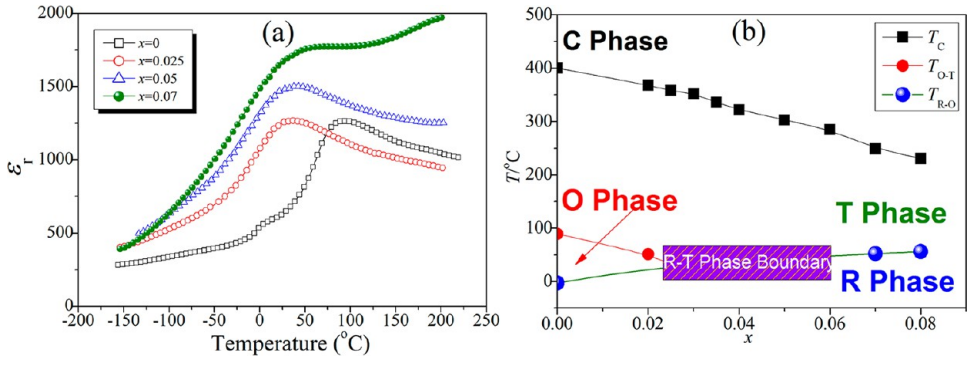

Figure 4. (a) Temperature (−150 to 200 °C) dependence of the dielectric constant and (b) the phase diagram of the KNLNS$_x$-BS ceramics.

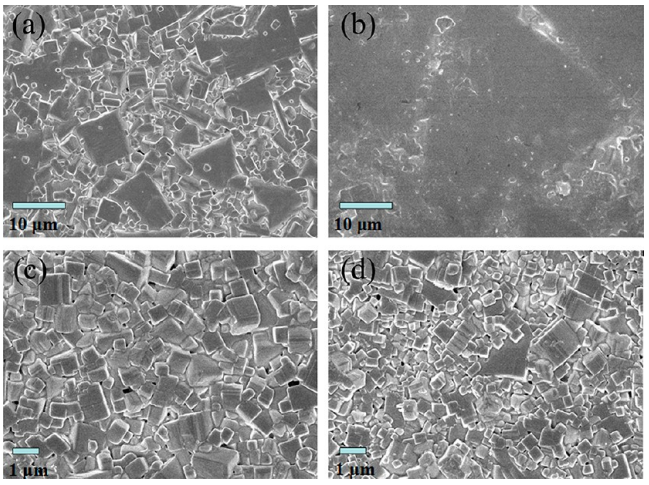

Figure 5. SEM micrographs of the KNLNS$_x$-BS ceramics: (a) x = 0, (b) x = 0.025, (c) x = 0.05, and (d) x = 0.07.

0.05. That is because that the smaller grains may fill up the gaps among the large ones for the ceramics with x = 0 and 0.025, while this process does not occur for the ceramics with x = 0.05 and 0.07, which gives rise to a poorer microstructure with some gaps. To show this point clearer, the relative density of the ceramics as a function of x is shown in Figure 6. One can see

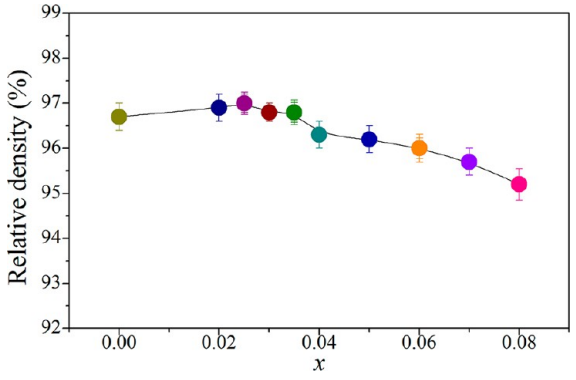

Figure 6. Relative density of the KNLNS$_x$-BS ceramics as a function of x.

that the relative density remains almost unchanged for the ceramics with x < 0.04, and it drops gradually as x further increases. In the present work, the distribution of each chemical element in the ceramic with x = 0.025 is characterized by the element mapping of the cross section of the sample using the energy-dispersive X-ray (EDX) analysis, and the results are shown in Figure 7. One can see that all the elements are homogeneously distributed in the ceramic. The Li element could not be detected using FE-SEM EDX technique because of its light weight.

To further appreciate the composition in large and small grains regions of the ceramic with x = 0.025, we have used the energy dispersion spectrum analysis (EDS) to reveal the atomic percentages of the elements within different regions. The results are shown in panels a and c in Figure 8 for smaller grains and panels b and d for larger grains. Panels e and f in Figure 8 show the atomic percentages of the elements, which is derived from panels c and d in Figure 8, respectively. Only a very small difference in the composition among the smaller and larger grain regions is observed, further indicating that the chemical compositions are homogeneously distributed in the ceramics. In addition, the Na/K ratio remains almost the same in these two different regions. In the following, the mechanism for the decrease in grain size of the ceramics with increasing the Sb content (x > 0.05) is given. Images a and b in Figure 9 show the composition analysis of a single grain and a large region containing many grains and grain boundaries in the ceramic with x = 0.05. It is observed that the Sc element is absent from the single grain, whereas it can be detected in the whole region of the ceramic. It has been reported that the grain growth is inhibited and the grain size decreases if Sc aggregates at the grain boundary.[38,39] Comparing Figure 8 with Figure 9, we conclude that the grain growth of the KNLNS$_x$-BS ceramics could be prohibited by the Sc ions located at grain boundaries and promoted by the Sc ions located in the grains.

Figure 10a shows the P-E hysteresis loops of the KNLNS$_x$-BS ceramics as a function of the Sb content, measured at 10 Hz and room temperature. A typical P–E loop is observed for all the ceramics, and the shape of P–E hysteresis loops varies with the Sb content. Figure 10(b) plots the variations of the remnant polarization (P_r) and the coercive field (E_C) with x. P_r slightly increases from 21.3 to 28.5 μC/cm^2 as x increases from 0 to 0.025, and then gradually drops as x increases further. E_C vs x shows a similar trend with P_r. E_C also rises first and then drops with increasing x, reaching the maximum value of ~21.0 kV/cm at x = 0.025. As a result, an enhanced ferroelectric behavior could be achieved in the R-T phase boundary region.

Figure 11a plots the P–E hysteresis loops of the KNLNS$_x$-BS ceramic with x = 0.025 measured at various temperatures of

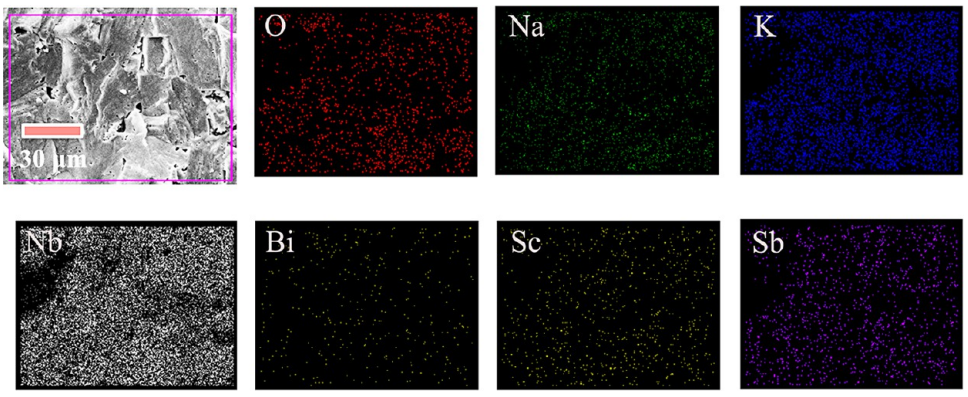

Figure 7. Elemental mapping of KNLNS$_x$-BS ceramics with x = 0.025.

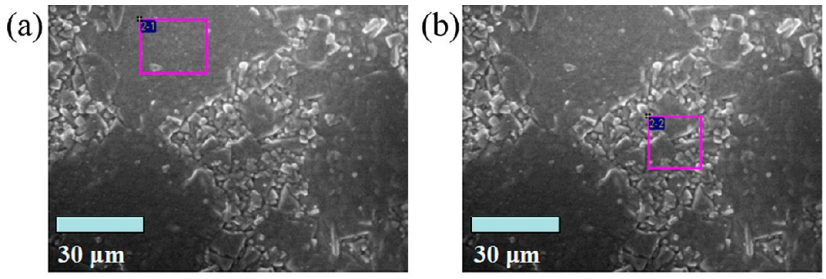

(e)

Element	Atomic (%)
O	55.63
Na	9.31
K	8.51
Sc	0.40
Nb	25.02
Sb	0.48
Bi	0.66

(f)

Element	Atomic (%)
O	57.74
Na	8.97
K	8.22
Sc	0.36
Nb	23.76
Sb	0.38
Bi	0.56

Figure 8. Surface morphologies of the ceramic with $x = 0.025$; (a) the region with small grains, (b) the region with large grains. (c, d) EDS spectra corresponding to the regions marked as 2−1 and 2−2 in a and b, respectively. (e, f) Atomic percentages of the elements obtained from c and d.

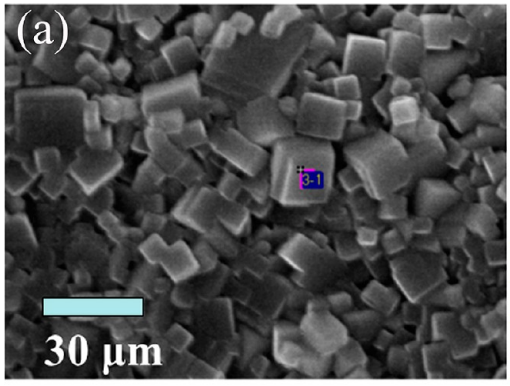

Element	Atom (%)	Element	Element (%)
O	56.14	Nb	24.37
Na	9.19	Sb	0.93
K	8.73	Bi	0.64

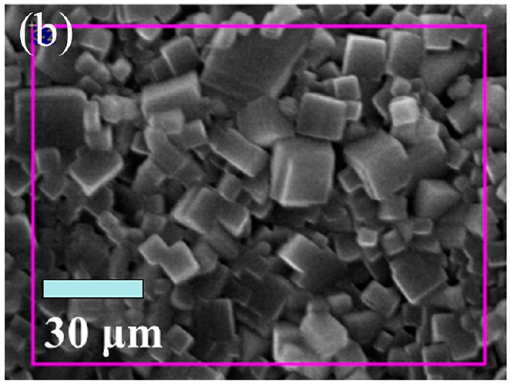

Element	Atom (%)	Element	Element (%)
O	60.40	Nb	21.50
Na	8.71	Sb	1.00
K	7.54	Bi	0.48
Sc	0.37		

Figure 9. Surface morphologies, EDS spectra, and atomic percentages of the elements of (a) a single grain and (b) the region of the ceramic with $x = 0.05$ containing many grains.

30−180 °C. A typical P−E loop is observed for the ceramics regardless of the measurement temperatures. The P−E loops show very weak temperature dependence, confirming a good temperature stability of the ferroelectric properties. We show

dx.doi.org/10.1021/am403448r | ACS Appl. Mater. Interfaces 2013, 5, 10409−10417

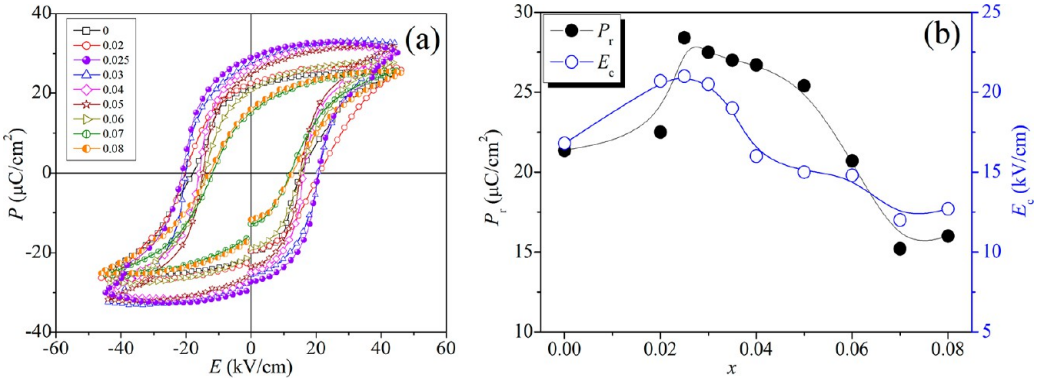

Figure 10. (a) *P*–*E* loops and (b) the profiles showing P_r and E_c vs the Sb content of the KNLNS$_x$-BS ceramics.

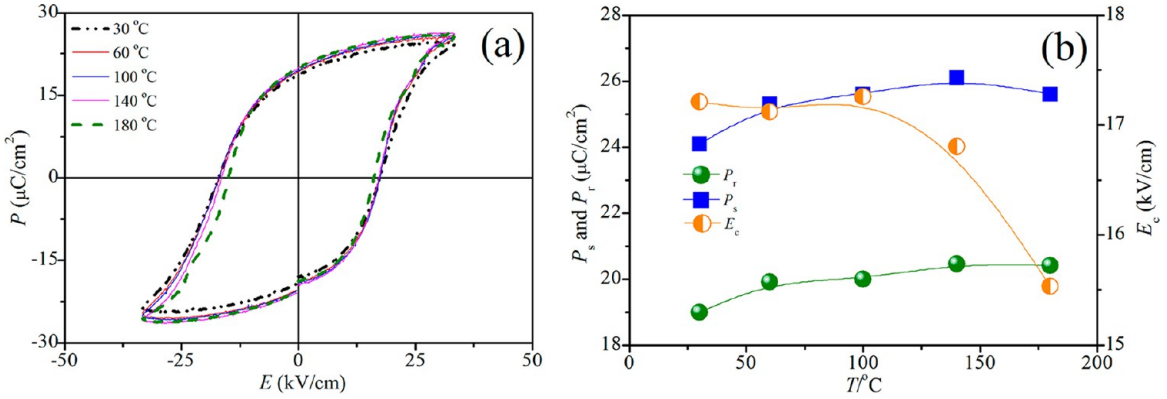

Figure 11. (a) Temperature -dependent *P*–*E* loops and (b) P_s, P_r, and E_c of the ceramic with x = 0.025.

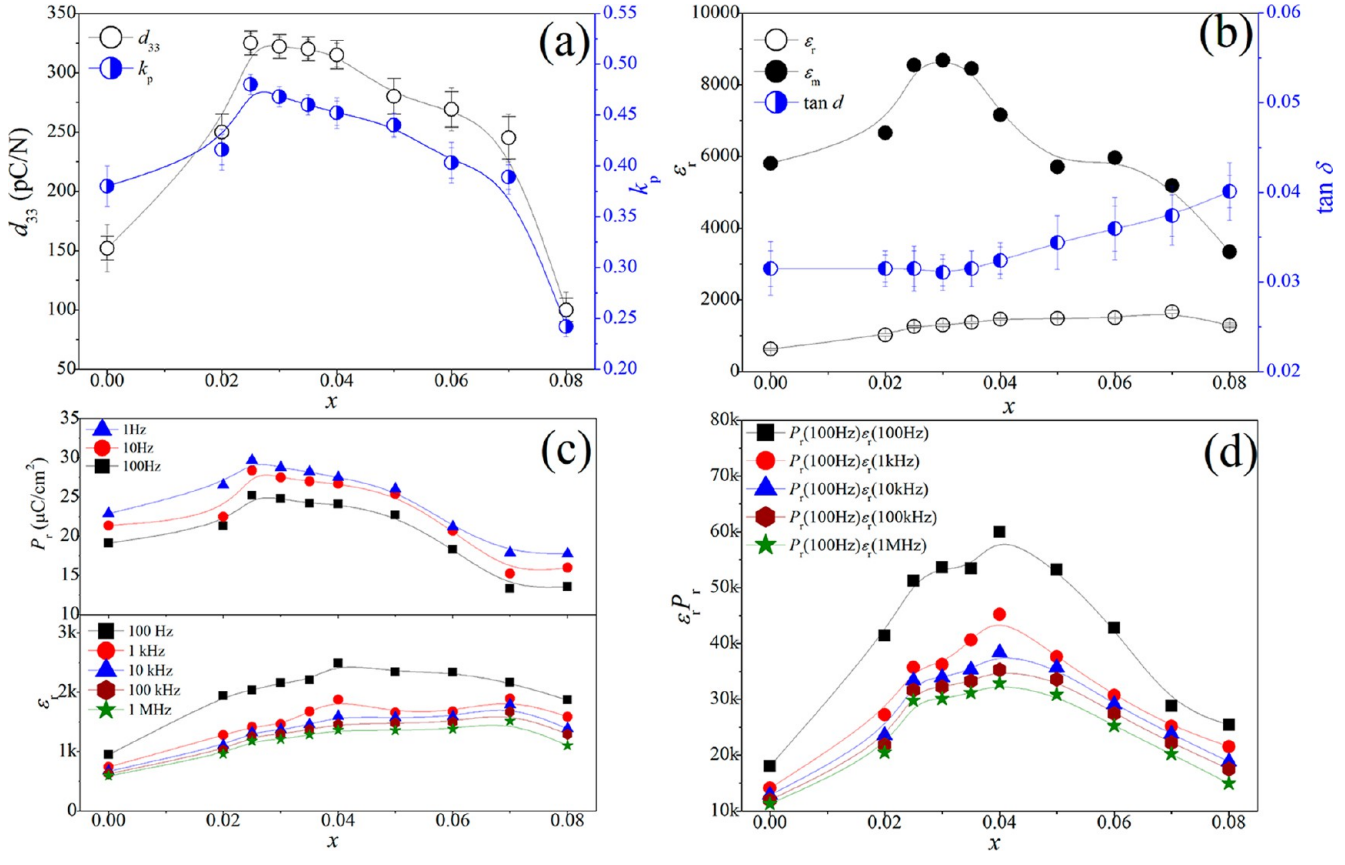

Figure 12. (a) d_{33}, k_p, (b) dielectric properties, (c) ε_r, P_r vs x, and (d) $\varepsilon_r P_r$ vs x of the KNLNS$_x$-BS ceramics.

Table 2. Electrical Properties of KNN-Based Ceramics

material system	d_{33} (pC/N)	k_p	T_c (°C)	phase boundary	ref
$(K_{0.5-x/2}Na_{0.5-x/2}Li_x)NbO_3$ [x = 0.065]	250	0.44	450	O-T	Hollenstein[40]
$(Na_{0.5}K_{0.5})_{1-x}(LiSb)_xNb_{1-x}O_3$	260	0.50	390	O-T	Zang[41]
$(K_{0.45}Na_{0.55})_{0.98}Li_{0.02}(Nb_{0.77}Ta_{0.18}Sb_{0.05})O_3$	413	0.50	~225	O-T	Gao[43]
$(Na_{0.5}K_{0.5})_{0.975}Li_{0.025}Nb_{0.76}Sb_{0.06}Ta_{0.18}O_3$	352	0.47	~210	O-T	Du[44]
$(Na_{0.52}K_{0.40})(Nb_{0.84}Sb_{0.08})O_3-LiTaO_3-BaZrO_3$	365	0.45	−180	R-T	Zuo[45]
$(1-x)K_{0.5}Na_{0.5}Nb_{1-x}Sb_xO_3$-$xBi_{0.5}Na_{0.5}TiO_3$	380	0.35	267	R-T	Liang[46]
$0.96(K_{0.5}Na_{0.5})_{0.95}Li_{0.05}Nb_{0.93}Sb_{0.07}O_3-0.04BaZrO_3$	425	0.50	197	R-T	Wu[47]
$0.992(K_{0.46}Na_{0.54})_{0.965}Li_{0.035}Nb_{1-x}Sb_xO_3-0.008BiScO_3$	325	0.48	~358	R-T	this work

the variation in ferroelectric properties with temperatures in a clearer manner, P_s, P_r, and E_c, obtained from Figure 11a, in Figure 11b. One can see that P_s and P_r increase slightly, while E_c decreases a little as temperature rises.

Figure 12a plots the room-temperature piezoelectric constant (d_{33}) and planar electromechanical coupling factor (k_p) of the KNLNS$_x$-BS ceramics as a function of the Sb content. We can see that piezoelectric properties of the KNLNS$_x$-BS ceramics demonstrate strong composition dependence. The piezoelectric properties can be enhanced by doping a small amount of Sb into KNLN-BS, and then be suppressed as the Sb content further increases. For the pure KNLN-BS ceramic, it shows a piezoelectric behavior of $d_{33} \approx 152$ pC/N and $k_p \approx 38.0\%$. For $x = 0.025$, both d_{33} and k_p reach the maximum values of 325 pC/N and 48%, respectively. As a result, the piezoelectric properties peak in the R-T phase boundary zone. In this work, the d_{33} is much larger than those obtained from other KNN-based ceramics containing $BiScO_3$,[26−30] as indicated in Table 1. In addition, the d_{33} of this work is also superior to those KNN-based[40−42] and PZT1 ceramics, as shown in Table 2 and Figure 13. Although its d_{33} is inferior to some of those KNN-based

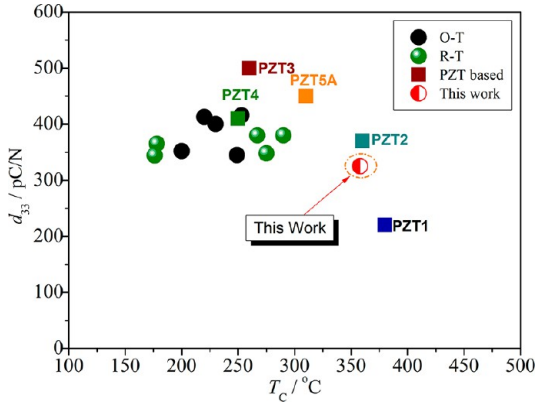

Figure 13. Schematic diagram summarizing d_{33} and T_c of high-performance KNN and PZT-based ceramics.

ceramics with O-T and R-T phase boundaries[43−47] or PZT-based ceramics, a much higher T_C (~358 °C) has been obtained in the current work, which is comparable to PZT2 (~360 °C) and is even higher than PZT3, PZT4, and PZT5A,[1,2] as shown in Figure 13. It is well-known that it is difficult to mediate the conflict between d_{33} and T_C in KNN.[26−31,37−42] In other words, the enhancement in d_{33} is normally obtained by sacrificing its T_C, and vice versa. In this work, an enhanced comprehensive performance of both a large d_{33} (~325 pC/N) and a high T_C (~358 °C) is achieved in such a material system with $x = 0.025$, which even compete with that of PZT2. Therefore, we have successfully realized the objective of obtaining a large d_{33} and a high T_C, widening the application temperature range of lead-free piezoelectric devices. Figure 12(b) plots the dielectric properties (ε_r, ε_m, and tan δ) of the KNLNS$_x$-BS ceramics as a function of the Sb content, measured at 100 kHz and room temperature. In this work, ε_m stands for the maximum value of dielectric constant in Figure 3. The ε_r increases as x increases and then drops for $x > 0.07$. tan δ of the ceramics remains almost unchanged for $x < 0.04$ and then gradually increases as the Sb content rises because of the formation of pores (see Figure 5), which is in agreement with the change in the relative density (Figure 6). In addition, ε_m exhibits a different trend, in which the maximum value is reached at $x = 0.025$, showing the involvement of a similar MPB.[13,48] The underlying physical mechanisms for the enhanced piezoelectric properties are discussed as follows: The involvement of two thermodynamically equivalent phases (R and T) results in the formation of highly oriented domains during the poling process,[49,50] and therefore the formation of the R-T phase coexistence must largely contribute to the enhanced piezoelectric properties of the ceramic with $x = 0.025$ in this work. The frequency dependence of ε_r and P_r of the KNLNS$_x$-BS ceramics were measured, and the results are shown in Figure 12c. It was found that a similar trend is observed for all the curves, which is independent of measurement frequencies. To show the combination effect of P_r and ε_r measured at different frequencies, we plotted the $\varepsilon_r P_r$ of KNLNS$_x$-BS ceramics as a function of x in Figure 12d, according to the results in Figure 12c. It can be clearly seen that all the $\varepsilon_r P_r$ vs x curves show the similar trend. In addition, we can see that a larger $\varepsilon_r P_r$ is observed in the vicinity of the R-T phase boundary region. Here, we argue that the enhanced $\varepsilon_r P_r$ is also partly responsible for the large d_{33} observed in this work.[35,46] As a result, the optimal dielectric and piezoelectric properties are achieved in the ceramic with $x = 0.025$, and the key parameters obtained are as follows: $d_{33} \approx 325$ pC/N, $k_p \approx 0.48$, $\varepsilon_r \approx 1257$, and tan $\delta \approx 0.031$.

It is important to study the thermal stability of a piezoelectric material because it may strongly affect the temperature range during practical applications.[51] It is well-known that d_{33} of a polarized piezoelectric ceramics drops gradually as the temperature increases ($\leq T_C$) because of the thermal instability of the polarization.[52] To evaluate the thermal stability of the KNLNS$_x$-BS ceramics developed in this work, the d_{33} of the polarized samples was characterized at different annealing temperatures (T_a), as plotted in Figure 14. Clearly, one see that the thermal stability of the KNLNS$_x$-BS ceramics is strongly affected by the Sb content, that is, the thermal stability gradually degrades as the Sb level increases. For $x = 0$, d_{33} shows a plateau below T_C. However, d_{33} decreases almost linearly with temperatures for the ceramics with $x > 0.05$. One can also see that the d_{33} of the ceramics with $x = 0.025-0.035$

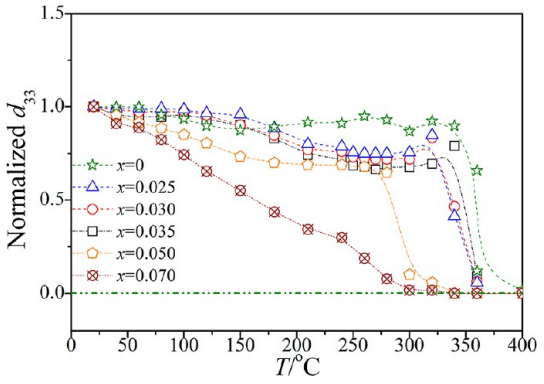

Figure 14. Thermal stability of the KNLNS$_x$-BS ceramics as a function of x.

levels off below 150 °C, and then slightly drops with further increasing T_a (150−240 °C). The profile becomes stable again up to 320 °C, and the dramatic decrease occurs when the T_a is near T_C. Note that there is no phase transition at ∼150 °C in the ceramics studied in this work. So, the reduction in d_{33} (>150 °C) is not caused by a phase transition.[52] It was reported that the defect dipoles may be responsible for the reduction of d_{33} upon annealing.[53] Since the piezoelectric properties of a ferroelectric material are strongly affected by the movement of the domain wall,[54,55] the defect dipoles prohibiting the movement of the domain wall may result in a stable d_{33} at a low annealing temperature (≤150 °C). As the annealing temperature increases (150−240 °C), the defect dipoles are decoupled, giving rise to the rearrangement of the domain structure and form a lower-energy configuration with a lower net polarization. This phenomenon may lead to the drop in d_{33} in this temperature regime (150−240 °C). The defect dipoles were totally decoupled and randomized when temperature increases up to 250 °C. So, d_{33} becomes stable again with a further increase in temperature up to T_c. As a result, the change in the domain-wall activities, induced by the change in the configuration of defect dipoles, results in the variation in the d_{33} with different annealing temperatures.[55,56]

CONCLUSION

Lead-free $0.992(K_{0.46}Na_{0.54})_{0.965}Li_{0.035}Nb_{1-x}Sb_xO_3$-$0.008BiScO_3$ piezoelectric ceramics have been prepared using the conventional solid-state method. The rhombohedral-tetragonal phase boundary was found to significantly enhance the piezoelectricity of the ceramics. A high T_C is also achieved by fine-tuning the composition of the material system. In this work, an optimal electrical behavior of $d_{33} \approx 325$ pC/N, $k_p \approx 48\%$, and $T_C \approx 358$ °C has been obtained in the ceramic with $x = 0.025$. The variation in the domain-wall activities, which is induced by the change in the configuration of defect dipoles upon annealing, results in a large change in the piezoelectric constant with increasing temperatures. It is expected that this material system is a promising candidate for the piezoelectric applications.

AUTHOR INFORMATION

Corresponding Author

*E-mail: msewujg@scu.edu.cn and wujiagang0208@163.com.

Notes

The authors declare no competing financial interest.

ACKNOWLEDGMENTS

The authors gratefully acknowledge the supports of the National Science Foundation of China (NSFC 51102173, 51272164, 51332003, and 51372195), the Introduction of Talent Start Funds of Sichuan University (2082204144033), and the Fundamental Research Funds for the Central Universities (2012SCU04A01).

REFERENCES

(1) Jaffe, B.; Cook, W. R.; Jaffe, H. *Piezoelectric Ceramics*; Academic Press: London, 1971.
(2) Jaffe, B.; Roth, R. S.; Marzullo, S. *J. Res. Natl Bur. Stand.* **1955**, *55*, 239−254.
(3) Bellaiche, L.; García, A.; Vanderbilt, D. *Phys. Rev. Lett.* **2000**, *84*, 5427−5430.
(4) Baettig, P.; Schelle, C. F.; Lesar, R.; Waghmare, U. V.; Spaldin, N. A. *Chem. Mater.* **2005**, *17*, 1376−1380.
(5) Zylberberg, J.; Belik, A. A.; Muromachi, E. T.; Ye, Z. G. *Chem. Mater.* **2007**, *19*, 6385−6390.
(6) Li, B. W.; Osada, M.; Ozawa, T. C.; Sasaki, T. *Chem. Mater.* **2012**, *24*, 3111−3113.
(7) Saito, Y.; Takao, H.; Tani, T.; Nonoyama, T.; Takatori, K.; Homma, T.; Nagaya, T.; Nakamura, M. *Nature* **2004**, *432*, 84−87.
(8) Takenaka, T.; Nagata, H. J. *Eur. Ceram. Soc.* **2005**, *25* (12), 2693−700.
(9) Rödel, J.; Kounga, A. B. N.; Weissenberger-Eibl, M.; Koch, D.; Bierwisch, A.; Rossner, W.; Hoffmann, M. J.; Danzer, R.; Schneider, G. J. *Eur. Ceram. Soc* **2009**, *29* (9), 1549−1560.
(10) Rödel, J.; Jo, W.; Seifert, K.; Anton, E. M.; Granzow, T.; Damjanovic, D. *J. Am. Ceram. Soc.* **2009**, *89*, 1153−1177.
(11) Shrout, T. R.; Zhang, S. *J. Electroceram.* **2007**, *19*, 111−124.
(12) Damjanovic, D.; Klein, N.; Li, J.; Porokhonskyy, V. *Funct. Mater. Lett.* **2010**, *3*, 5−13.
(13) Liu, W.; Ren, X. *Phys. Rev. Lett.* **2009**, *103*, 257602.
(14) Wu, J.; Xiao, D.; Wu, W.; Chen, Q.; Zhu, J.; Yang, Z.; Wang, J. *Scr. Mater.* **2011**, *65*, 771−774.
(15) Takenaka, T.; Maruyama, K.; Sakata, K. *Jpn. J. Appl. Phys., Part 1* **1991**, *30* (9B), 2236−2239.
(16) Lin, D.; Xiao, D.; Zhu, J.; Yu, P. *Appl. Phys. Lett.* **1991**, *88*, 062901.
(17) Zhang, S. T.; Kounga, A. B.; Aulbach, E.; Jo, W.; Granzow, T.; Ehrenberg, H.; Rödel, J. *J. Appl. Phys.* **2008**, *103* (3), 034108.
(18) Guo, Y.; Kakimoto, K.; Ohsato, H. *Appl. Phys. Lett.* **2004**, *85*, 4121−4123.
(19) Zhang, S.; Xia, R.; Shrout, T. R. *J. Electroceram.* **2007**, *19* (4), 251−257.
(20) Zhang, S.; Xia, R.; Hao, H.; Liu, H.; Shrout, T. R. *Appl. Phys. Lett.* **2008**, *92* (15), 152904.
(21) Zuo, R. Z.; Rödel, J.; Chen, R. Z.; Li, L. T. *J. Am. Ceram. Soc.* **2006**, *89* (6), 2010−2015.
(22) Matsubara, M.; Yamaguchi, T.; Kikuta, K.; Hirano, S. *Jpn. J. Appl. Phys., Part 1* **2005**, *44* (8), 6136−6142.
(23) Wu, J. G.; Xiao, D. Q.; Wang, Y. Y.; Zhu, J. G.; Wu, L.; Jiang, Y. H. *Appl. Phys. Lett.* **2007**, *91* (25), 252907.
(24) Du, H.; Zhou, W.; Luo, F.; Zhu, D.; Qu, S.; Li, Y.; Pei, Z. *J. Phys. D: Appl. Phys.* **2008**, *41*, 085416.
(25) Park, H. Y.; Cho, K. H.; Paik, D. S.; Nahm, S.; Lee, H. G.; Kim, D. H. *J. Appl. Phys.* **2007**, *102*, 124101.
(26) Zuo, R. Z.; Ye, C.; Fang, X. S. *Jpn. J .Appl. Phys* **2007**, *46* (10A), 6733−6736.
(27) Li, X.; Jiang, M.; Liu, J.; Zhu, J.; Zhu, X.; Zhu, J.; Xiao, D. *J. Am. Ceram. Soc.* **2009**, *92* (7), 1625−1628.
(28) Jiang, M.; Deng, M.; Lu, H.; Wang, S.; Liu, X. *Mater. Sci. Eng., B* **2011**, *176*, 167−170.
(29) Wang, M.; Zhu, J.; Liu, J.; Zhu, B.; Li, X.; Sun, P.; Zhu, X.; Zhu, J.; Xiao, D. *Jpn. J. Appl. Phys.* **2011**, *50*, 120207.
(30) Li, X.; Zhu, J.; Wang, M.; Luo, Y.; Shi, W.; Li, L.; Zhu, J.; Xiao, D. *J. Alloys Compd.* **2010**, *499*, L1−L4.

(31) Sun, X.; Deng, J.; Sun, C.; Li, J.; Chen, J.; Yu, R.; Liu, G.; Xing, X.; Qiao, L. *J. Am. Ceram. Soc.* **2009**, *92* (8), 1853−1855.
(32) Belik, A. A.; Iikubo, S.; Kodama, K.; Igawa, N.; Shamoto, S.; Maie, M.; Nagai, T.; Matsui, Y.; Stefanovich, S.; Bogdan, I.; Lazoryak, I.; Takayama-Muromachi, E. *J. Am. Chem. Soc.* **2006**, *128*, 706−707.
(33) Eitel, R. E.; Randall, C. A.; Shrout, T. R.; Rehrig, P. W.; Hackenberger, W.; Park, S. E. *Jpn. J. Appl. Phys., Part 1* **2001**, *40*, 5999−6002.
(34) Zuo, R. Z.; Fu, J.; Lv, D. Y. *J. Am. Ceram. Soc.* **2010**, *93* (9), 2783−2787.
(35) Cheng, X.; Wu, J.; Wang, X.; Zhang, B.; Zhu, J.; Xiao, D.; Wang, X.; Lou, X. *Appl. Phys. Lett.* **2013**, *103*, 052906.
(36) Wu, J.; Wang, Y.; Xiao, D.; Zhu, J.; Yu, P.; Wu, L.; Wu, W. *Jpn. J. Appl. Phys.* **2007**, *46*, 7375−7377.
(37) Shannon, R. D. *Acta Cryst. A* **1976**, *32*, 751−67.
(38) Xin, C. R.; Zhang, J.; Liu, Y.; Zhang, Q. L.; Yang, H.; Cheng, D. *Mater. Res. Bull.* **2013**, *48*, 2220−2226.
(39) Coondoo, I.; Panwar, N.; Bdikin, I.; Puli, V. S.; Katiyar, R. S.; Kholkin, A. L. *J. Phys. D: Appl. Phys.* **2012**, *45*, 055302.
(40) Hollenstein, E.; Davis, M.; Damjanovic, D.; Setter, N. *Appl. Phys. Lett.* **2005**, *87*, 182905.
(41) Zang, G. Z.; Wang, J. F.; Chen, H. C.; Su, W. B.; Wang, C. M.; Qi, P.; Ming, B. Q.; Du, J.; Zheng, L. M.; Zhang, S.; Shrout, T. R. *Appl. Phys. Lett.* **2006**, *88*, 212908.
(42) Chang, Y. F.; Yang, Z.; Ma, D.; Liu, Z.; Wang, Z. *J. Appl. Phys.* **2008**, *104*, 024109.
(43) Gao, Y.; Zhang, J.; Qing, Y.; Tan, Y.; Zhang, Z.; Hao, X. *J. Am. Ceram. Soc.* **2011**, *94* (9), 2968−2973.
(44) Du, J.; Wang, J.; Zang, G.; Yi, X. *Physica B* **2011**, *406*, 4077−4079.
(45) Zuo, R.; Fu, J. *J. Am. Ceram. Soc.* **2011**, *94*, 1467−1470.
(46) Liang, W. F.; Wu, W. J.; Xiao, D. Q.; Zhu, J. G.; Wu, J. G. *J. Mater. Sci.* **2011**, *46*, 6871−6876.
(47) Zhang, B.; Wu, J.; Cheng, X.; Wang, X.; Xiao, D.; Zhu, J.; Wang, X.; Lou, X. *ACS Appl. Mat. Interfaces* **2012**, *4* (3), 1182−1185.
(48) Wu, J.; Xiao, D.; Wu, W.; Chen, Q.; Zhu, J.; Yang, Z.; Wang, J. *J. Eur. Ceram. Soc.* **2012**, *32*, 891−898.
(49) Benguigui, L. *Solid State Commun.* **1972**, *11*, 825−828.
(50) Haertling, G. H. *J. Am. Ceram. Soc.* **1999**, *82* (4), 797−818.
(51) Chen, S.; Dong, X.; Mao, C.; Cao, F. *J. Am. Ceram. Soc.* **2006**, *89* (10), 3270−3272.
(52) Ge, H.; Hou, Y.; Rao, X.; Zhu, M.; Wang, H.; Yan, H. *Appl. Phys. Lett.* **2011**, *99*, 032905.
(53) Zeng, T.; Yan, H.; Reece, M. J. *J. Appl. Phys.* **2010**, *108*, 096101.
(54) Zhang, Q. M.; Wang, H.; Kim, N.; Cross, L. E. *J. Appl. Phys.* **1994**, *75*, 454−459.
(55) Damjanovic, D.; Demartin, M.; Shulman, H. S.; Testorf, M.; Setter, N. *Sens. Actuators A* **1996**, *53*, 353−360.
(56) Yan, H.; Zhang, H.; Reece, M. J.; Dong, X. *Appl. Phys. Lett.* **2005**, *87*, 082911.